Transient versus Static Electron Spin Relaxation in Mn^{2+} Complexes Relevant as MRI Contrast Agents

Carlos Platas-Iglesias[*a], David Esteban-Gómez[a], Lothar Helm[b], and Martín Regueiro-Figueroa[a]

[a] Centro de Investigaciones Científicas Avanzadas (CICA) and Departamento de Química Fundamental, Universidade da Coruña, Campus da Zapateira, Rúa da Fraga 10, 15008 A Coruña, Spain

[b] Laboratoire de Chimie Inorganique et Bioinorganique, Ecole Polytechnique Fédérale de Lausanne, EPFL-BCH, CH-1015 Lausanne, Switzerland

The Journal of Physical Chemistry A Volume 120, Issue 32, pages 6467–6476, August 18, 2016
Received: 30 May 2016, Published online: 26 July 2016, Published in print: 18 August 2016

How to cite:

Transient versus Static Electron Spin Relaxation in Mn2+ Complexes Relevant as MRI Contrast Agents. Carlos Platas-Iglesias, David Esteban-Gómez, Lothar Helm, and Martín Regueiro-Figueroa *The Journal of Physical Chemistry A* **2016** *120* (32), 6467-6476. DOI: 10.1021/acs.jpca.6b05423

Abstract

The zero-field splitting (ZFS) parameters of the $[Mn(EDTA)(H_2O)]^{2-}\cdot 2H_2O$ and $[Mn(MeNO2A)(H_2O)]\cdot 2H_2O$ systems were estimated by using DFT and *ab initio* CASSCF/NEVPT2 calculations (EDTA = 2,2′,2″,2‴-(ethane-1,2-diylbis(azanetriyl))tetraacetate; MeNO2A = 2,2′-(7-methyl-1,4,7-triazonane-1,4-diyl)diacetate). Subsequent molecular dynamics calculations performed within the atom-centered density matrix propagation (ADMP) approach provided access to the transient and static ZFS parameters, as well as to the correlation time of the transient ZFS. The calculated ZFS parameters present a reasonable agreement with the experimental values obtained from the analysis of ^1H relaxation data. The correlation times calculated for the two systems investigated turned out to be very short ($\tau_c \sim 0.02–0.05$ ps), which shows that the transient ZFS is modulated by molecular vibrations. On the contrary, the static ZFS is modulated by the rotation of the complexes in solution, which for the small complexes investigated here is characterized by rotational correlation times of $\tau_R \sim 35–60$ ps. As a result, electron spin relaxation in small Mn^{2+}complexes is dominated by the static ZFS.

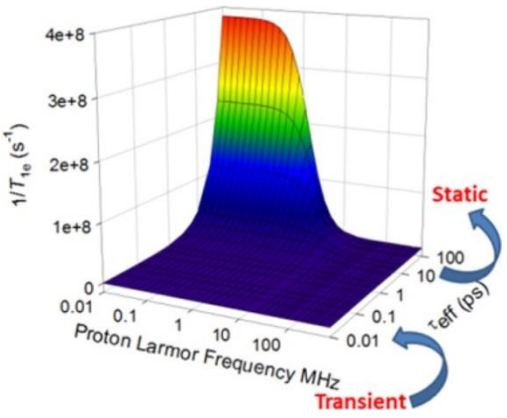

Keywords: contrast agents; coordination compounds; manganese; human serum albumin; NMR imaging

Introduction

Contrast agents (CAs) for magnetic resonance imaging (MRI) are generally paramagnetic substances that increase image contrast by reducing the longitudinal and/or transverse relaxation times of ^{1}H nuclei of water molecules in the vicinity of the agent.[1,2] Most of the CAs approved for clinical use are Gd^{3+} complexes with polyaminopolycarboxylate ligands that ensure a high stability of the complex in solution, while leaving a vacant coordination position that occupies a water molecule.[3-5] The Gd^{3+} ion was chosen as the ideal candidate for this purpose due to its slow electron spin relaxation time associated with the symmetric ^{8}S electronic ground state.[6]

High-spin Mn^{2+} complexes represent an attractive alternative to the clinically available Gd^{3+}-based agents due to their potential lower toxicity.[7,8] For instance, the CA mangafodipir trisodium, (Na_3[Mn(DPDP)], TESLASCAN, see Scheme 1), has been used as a hepatocyte specific MRI contrast agent.[9] Besides, the toxicity associated with the administration of some CAs based on Gd^{3+} [10,11] has triggered a renewed interest in Mn^{2+} agents.[12-15] Furthermore, the recent development of fast field-cycling MRI scanners has made it possible to improve image contrast by taking advantage of the high values and rapid variation of the relaxivity of Mn^{2+} complexes below 0.5 T.[16]

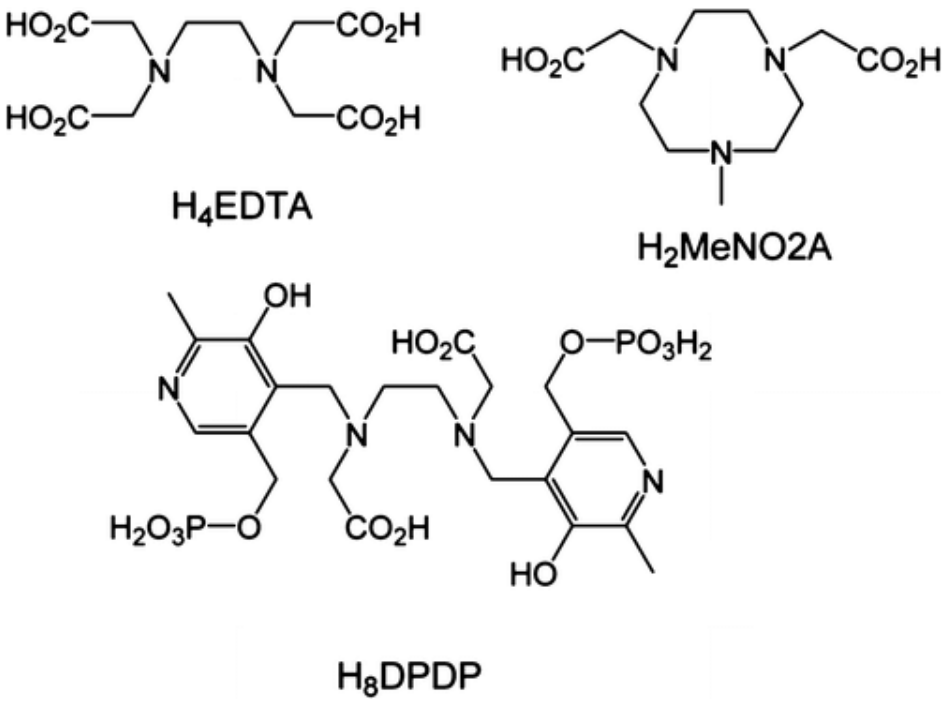

Scheme 1. Ligands Discussed in the Present Work.

The efficiency of a Mn^{2+}-based CA to enhance the relaxation rates of water proton nuclei is often interpreted by using the Solomon–Bloembergen–Morgan[17-20] theory for inner-sphere relaxation and the Freed model for the outer-sphere contribution.[21] The inner-sphere contribution depends upon structural parameters such as the number of water molecules coordinated to the metal ion (q) and the distance between the metal ion and the inner-sphere water proton nuclei. Additionally, four correlation times play key roles in the relaxation efficiency of the CA: the residence time of water protons in the metal coordination sphere (τ_m), the rotational correlation time of the Mn···H vector (τ_R), and the longitudinal and transverse electronic relaxation times of the metal ion ($T_{1e}$and T_{2e}). For decades, both T_{1e} and T_{2e} were assumed to be the result of fluctuations of a transient zero-field splitting (ZFS) Hamiltonian.[22] However, different groups have pointed out that the static

ZFS Hamiltonian should also provide an important source of electronic relaxation, at least in the case of Gd^{3+} complexes.[23-26]

The correlation time for the transient ZFS τ_v in Gd^{3+} complexes was estimated to be ~1 ps by Fries et al.[27] from the analysis of EPR spectra, whereas Pollet et al.[28] obtained a value of ~0.1 ps using *ab initio* molecular dynamics. However, the magnitude of τ_v for Mn^{2+} complexes has not yet been estimated experimentally or computationally. In recent papers, we showed that DFT calculations coupled to molecular dynamics studies based on the atom centered density matrix propagation (ADMP) model provide a straightforward access to ^{17}O hyperfine coupling constants of $[Mn(H_2O)_6]^{2+}$, $[Mn(EDTA)(H_2O)]^{2-}$, and [Mn(MeNO2A)(H_2O)] (Scheme 1).[29,30] Furthermore, a combined analysis of the ^1H nuclear magnetic relaxation dispersion (NMRD) profiles and ^{17}O NMR chemical shifts and relaxation rates provided experimental values of the zero-filed splitting energy. Thus, herein we extend these studies to investigate the ZFS energies in $[Mn(EDTA)(H_2O)]^{2-}$ and [Mn(MeNO2A)(H_2O)], as well as the fluctuation of the ZFS along the trajectories calculated using ADMP molecular dynamics.

Computational Details

The geometries of the $[Mn(EDTA)(H_2O)]^{2-}\cdot 2H_2O$ and $[Mn(MeNO2A)(H_2O)]\cdot 2H_2O$ systems optimized in aqueous solution at the TPSSh/SVP[31,32] level were described in our previous works.[30] Classical trajectory calculations were performed in aqueous solution at the TPSSh/SVP level by using the atom-centered density matrix propagation (ADMP) molecular dynamics model.[33-35] ADMP calculations on the $[Mn(EDTA)(H_2O)]^{2-}\cdot 2H_2O$ and $[Mn(MeNO2A)(H_2O)]\cdot 2H_2O$ systems were performed in aqueous solution using time steps of 0.2 fs, whereas a total of 7000 steps were run for the trajectory simulations. The fictitious electron mass was 0.1 amu. All the ADMP calculations were started from the corresponding optimized geometries obtained as described above. Bulk solvent effects were included by using the integral equation formalism variant of the polarizable continuum model (IEFPCM),[36] in which the solute cavity is built as an envelope of spheres centered on atoms or atomic groups with appropriate radii. The universal force field radii (UFF)[37] scaled by a factor of 1.1 were used to define the solute cavities. ADMP simulations in combination with polarized continuum models were shown to provide good results for the prediction of magnetic parameters (hyperfine tensors and **g**-tensors) that are tuned by short-time dynamical effects.[38] The ADMP approach provides O(*N*) scaling with computational time (*N* being the number of electrons),[39] making it a reasonable choice compared to computationally more expensive ab initio molecular dynamics methods (i.e., Born–Oppenheimer molecular dynamics, BOMD).[40] These calculations were performed by employing the Gaussian 09 package (Revision D.01).[41]

ZFS parameters were calculated using the ORCA program package (Version 3.0.1)[42] and the methodology developed by Neese.[43] In these calculations we tested the popular B3LYP functional,[44,45] the nonhybrid variant of TPSSh, TPSS, and the TPSS0 functional, a 25% exchange version of TPSSh (10% exchange) that provides improved energetics.[46] The geometries of the complexes optimized with the Gaussian code as described above were employed for the calculation of ZFS parameters. The TZVP basis set of Ahlrichs and colleagues was used in these calculations.[47] The RIJCOSX approximation[48-51] was used to speed up calculations of the ZFS parameters using the Def2-TZVPP/JK[52] auxiliary basis set as constructed automatically by ORCA. The spin–orbit contribution was considered employing the spin–orbit mean field approach (SOMF) using the one-center approximation to the exchange term (SOMF(1X)).[53] The convergence tolerances and integration accuracies of the calculations were increased from the defaults using the available TightSCF and Grid5 options. Solvent effects (water) were taken into account by using the conductor-like screening model (COSMO) as implemented in ORCA.[54] Nonrelativistic energy levels and wave functions were computed using the complete active space self-consistent field (CASSCF) method[55] along with the TZVP basis set and the COSMO solvation model. CASSCF calculations were

performed by using an active space including five electrons distributed into the five Mn 3d-based molecular orbitals (CAS(5,5)). The orbitals were optimized by the average of 1 sextet, 24 quartet, and 75 doublet roots. The ZFS parameters were subsequently calculated on the CASSCF wave functions using *N*-electron valence perturbation theory to second order (NEVPT2),[56-59] which computes the energies and wave functions of all magnetic sublevels by diagonalization of the full SOC matrix.

Results and Discussion

Model Systems

The geometries of the $[Mn(EDTA)(H_2O)]^{2-}\cdot 2H_2O$ and $[Mn(MeNO2A)(H_2O)]\cdot 2H_2O$ systems (Figure 1) optimized in aqueous solution at the TPSSh/SVP level are presented in Figure 1. Our previous studies showed that the explicit inclusion of at least two second sphere water molecules is critical to obtain accurate $Mn–O_{water}$ distances and ^{17}O hyperfine coupling constants. In the case of $[Mn(EDTA)(H_2O)]^{2-}\cdot xH_2O$ the $Mn–O_{water}$ distance decreases from 2.56 to 2.26 Å as x increases from 0 to 2, whereas the calculated ^{17}O hyperfine coupling constants vary from −2.60 to −6.47 MHz (experimental value −6.45 MHz).[30] For $[Mn(MeNO2A)(H_2O)]\cdot xH_2O$ the $Mn–O_{water}$ distance shortens from 2.29 to 2.16 Å upon inclusion of two second-sphere water molecules. The Mn^{2+} ion in $[Mn(EDTA)(H_2O)]^{2-}\cdot 2H_2O$ is seven-coordinated by the N_2O_4 donor set of the ligand and an oxygen atom of a coordinated water molecule, which results in a capped trigonal prismatic coordination environment. The metal coordination environment in $[Mn(MeNO2A)(H_2O)]\cdot 2H_2O$ is distorted octahedral.

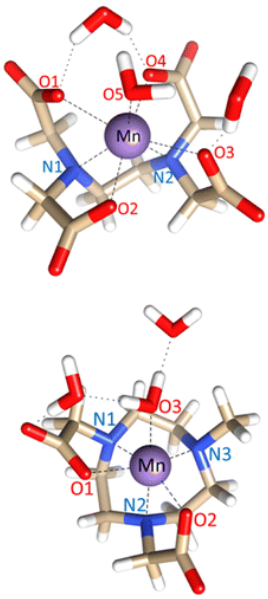

Figure 1. Optimized geometries of the $[Mn(EDTA)(H_2O)]^{2-}\cdot 2H_2O$ and $[Mn(MeNO2A)(H_2O)]\cdot 2H_2O$ systems calculated at the TPSSh/SVP level.

Zero-Field Splitting Calculations

The electronic ^6S ground state high-spin Mn^{2+} ion is characterized by an electronic spin state $S = 5/2$, which implies that the degeneracy of the magnetic sublevels $M_S = \pm 5/2, \pm 3/2$, and $\pm 1/2$ is broken in the absence of any applied magnetic field due to zero-field splitting effects.[60] The phenomenological ZFS Hamiltonian contains the nine components of the **D**-tensor and can be expressed as[60, 61]

$$\hat{H}_{\mathrm{ZFS}} = \hat{S}\mathbf{D}\hat{S} \tag{1}$$

Taking a coordinate system that diagonalizes the **D** tensor allows writing the ZFS Hamiltonian as

$$\hat{H}_{\mathrm{ZFS}} = D\left(\hat{S}_z^{\,2} - \frac{1}{3}\hat{S}^2\right) + E\left(\hat{S}_x^{\,2} - \hat{S}_y^{\,2}\right) \tag{2}$$

where *D* and *E* are the axial and rhombic ZFS parameters, which take the forms

$$D = D_{zz} - \frac{1}{2}\left(D_{xx} + D_{yy}\right) \tag{3}$$

$$E = \frac{1}{2}\left(D_{xx} - D_{yy}\right) \tag{4}$$

The *D* and *E* values are normally given in a coordinate system that fulfills the relationship

$$|D| \geq 3E \geq 0 \tag{5}$$

The ZFS parameters *D* and *E* of the energy-minimized structures of $[Mn(EDTA)(H_2O)]^{2-}\cdot 2H_2O$ and $[Mn(MeNO2A)(H_2O)]\cdot 2H_2O$ were calculated using four different functionals (B3LYP, TPSS, TPSSh, and TPSS0) in combination with the TZVP basis set. A systematic DFT study of ZFS parameters in Mn^{2+} complexes did not find any noticeable improvement of the calculated parameters using larger basis sets.[63] The calculated ZFS parameters are given in Table 1.

The results reported in Table 1 show that the calculated ZFS parameters vary significantly depending on the particular functional employed in the calculation. Generally, the nonhybrid TPSS functional provides smaller absolute *D* values than the hybrid B3LYP and TPSSh functionals. The TPSS0 functional was included in this investigation because it was found recently that it provides calculated **g**- and **A**-tensors in better agreement with the experimental EPR data than TPSSh.[64, 65] However, TPSS0 leads to rather erratic results in the present case. Overall, the results presented in Table 1 show that the ZFS parameters in Mn^{2+} complexes are rather difficult to predict with DFT, which is in line with previous studies that provided accuracies of ~0.1 cm^{-1}.[63] Thus, the ZFS parameters were also calculated using ab initio CASSCF/NEVPT2 calculations, which were shown to provide ZFS values of transition metal complexes in excellent agreement with the experiment.[66-68] The results show that among the different functionals explored in this work TPSS provides the best agreement with CASSCF/NEVPT2 calculations (Table 1).

Table 1. ZFS Parameters Obtained with DFT and CASSCF/NEVPT2 Calculations and Experimental Values Reported in the Literature.

ligand		D/cm^{-1}	E/D	Δ/cm^{-1}	$\Delta^2/10^{19}$ rad^2 s^{-2}
EDTA	B3LYP	−0.1064	0.3056	0.09832	34.3
	TPSS	−0.0405	0.2419	0.03585	4.56
	TPSSh	−0.1133	0.0291	0.09263	30.5
	TPSS0	−0.0487	0.0156	0.03980	5.62
	NEVPT2[c]	−0.0309	0.1376	0.0259	2.39
exp[a]				0.0418	6.19
MeNO2A	B3LYP	0.1168	0.2063	0.01025	37.3
	TPSS	0.0519	0.1422	0.0436	6.75
	TPSSh	0.0451	0.1042	0.0374	4.97
	TPSS0	−0.1347	0.0803	0.11107	43.8
	NEVPT2[c]	0.0452	0.1725	0.0385	5.26
exp[b]				0.0450	7.2

[a]From ref 62. [b]From ref 30. [c]Values obtained with NEVPT2 calculations using the CASSCF wave functions.

From the values of the axial and rhombic ZFS parameters the ZFS energy can be calculated according to

$$\Delta = \sqrt{\frac{2}{3}D^2 + 2E^2} \qquad (6)$$

The values of Δ obtained with DFT calculations compare reasonably well with those obtained experimentally from ^{1}H relaxometric studies (Table 1), the best agreement being provided by the TPSS functional. This is in line with recent results obtained for $[GdF_6]^{3-}$ and $[Gd(H_2O)_6]^{3+}$, which showed that hybrid functionals are less accurate than nonhybrid functionals when compared to CASSCF results, especially if a large amount of Hartree–Fock (HF) exchange is added to the functional.[69] This has been attributed in the case of Gd^{3+} complexes to an increase of the HOMO–LUMO gap upon increasing HF exchange.[69] A similar behavior is found for the Mn^{2+}complexes investigated in this work. For instance, the energy difference between the highest occupied and lowest unoccupied α orbitals in $[Mn(MeNO2A)(H_2O)]\cdot 2H_2O$ is 3.40, 4.65, and 7.39 eV for the TPSS, TPSSh, and TPSS0 functionals, respectively. The corresponding figures obtained for $[Mn(EDTA)(H_2O)]^{2-}\cdot 2H_2O$ are 4.39 (TPSS), 4.64 (TPSSh), and 6.55 eV (TPSS0).

It is important to note that the experimental ZFS parameters were obtained without separation of the static and transient contributions. However, the results reported in Table 1 indicate that our DFT calculations at the TPSS/TZVP level on the energy-minimized structures provide at least the correct order of magnitude of the ZFS in this family of compounds.

The ZFS is the result of a direct electron–electron magnetic dipole spin–spin (SS) interaction involving unpaired electrons and the spin–orbit coupling (SOC) of excited states into the ground state.[70] The calculated SS and SOC contributions to the ZFS parameters of the mononuclear systems investigated here indicate that

the *D* values originate basically from the SOC part (Table 2). The relative contributions of the four different types of excited states originating from α → α, β → β, α → β, and β → α excitations were found to vary significantly depending on the particular complex.

Table 2. Spin–Spin (SS) and Spin–Orbit Coupling (SOC) Contributions to the *D* Values [cm^{-1}] Calculated at the TPSS/TZVP Level

	D_{SS}	D_{SOC}	α → α	β → β	α → β	β → α
EDTA	0.0038	−0.044	−0.042	−0.039	0.010	0.027
MeNO2A	0.0094	0.042	−0.006	0.000	0.039	0.010

Molecular Dynamics Simulations

The correlation time for the transient ZFS in Gd^{3+} complexes was estimated to be ∼1 ps by Fries.[25,26] This time scale can be rather easily accessed by *ab initio* molecular dynamics methods. Previous studies on Gd^{3+} complexes showed that the transient ZFS is modulated by fast molecular vibrations.[28] Thus, we have carried out molecular dynamics simulations using the ADMP approach and a mixed cluster/continuum model.[71] These simulations were performed in solution at the TPSSh/SVP level starting on the optimized geometries. Our simulations performed on the $[Mn(MeNO2A)(H_2O)]\cdot 2H_2O$ system show that the bond distances of the metal coordination environment experience relatively important fluctuations during the length of the simulations (1.4 ps, Figure 2). The Mn–N distances fluctuate within the range 2.21–2.65 Å, whereas the Mn–O bonds oscillate between 1.94 and 2.27 Å. Similarly, fluctuations in the ranges 2.27–2.71 and 2.03–2.51 Å were observed for the Mn–N and Mn–O bonds in $[Mn(EDTA)(H_2O)]^{2-}\cdot 2H_2O$. The smaller average Mn–donor distances obtained for $[Mn(MeNO2A)(H_2O)]\cdot 2H_2O$ are expected due to the lower coordination number of the metal ion (CN = 6) when compared with that for $[Mn(EDTA)(H_2O)]^{2-}\cdot 2H_2O$ (CN = 7).

The static ZFS interaction is obtained by averaging over the fast processes occurring in solution (vibrations, collisions) and is modulated by rotation of the complex.[72] The ZFS tensor is a symmetric 3 × 3 matrix with the form[28]

$$D_{\mathrm{ZFS}} = \begin{pmatrix} d_{11} & d_{12} & d_{13} \\ d_{21} & d_{22} & d_{23} \\ d_{31} & d_{32} & d_{33} \end{pmatrix} \qquad (7)$$

The trajectories obtained from ADMP simulations were used to perform a configurational space sampling by taking snapshots at regular intervals of 12 fs. The ZFS tensor was subsequently calculated for each snapshot at the TPSS/TZVP level. The d_{ij} values calculated along the ADMP trajectories show nearly Gaussian distributions around their average values (Figure 3). We notice a broader distribution of the d_{ij} values for $[Mn(MeNO2A)(H_2O)]\cdot 2H_2O$ than for $[Mn(EDTA)(H_2O)]^{2-}\cdot 2H_2O$. The analysis of the d_{ij} parameters calculated for $[Mn(MeNO2A)(H_2O)]\cdot 2H_2O$ reveals weak linear relationships between the d_{ij} parameters, with Pearson's correlation coefficients of 0.57, 0.85, and 0.60 for the d_{11}/d_{22}, d_{11}/d_{33}, and d_{22}/d_{33} data pairs,

respectively (Figure 4). The linear relationship is even weaker for $[Mn(EDTA)(H_2O)]^{2-}\cdot 2H_2O$, the Pearson correlation coefficients being −0.03 (d_{11}/d_{22}), 0.18 (d_{11}/d_{33}), and 0.52 (d_{22}/d_{33}). The broader distribution and higher correlation of d_{ij} values in $[Mn(MeNO2A)(H_2O)]\cdot 2H_2O$ might be related to a more important rigidity of the complex associated with the macrocyclic nature of the ligand.

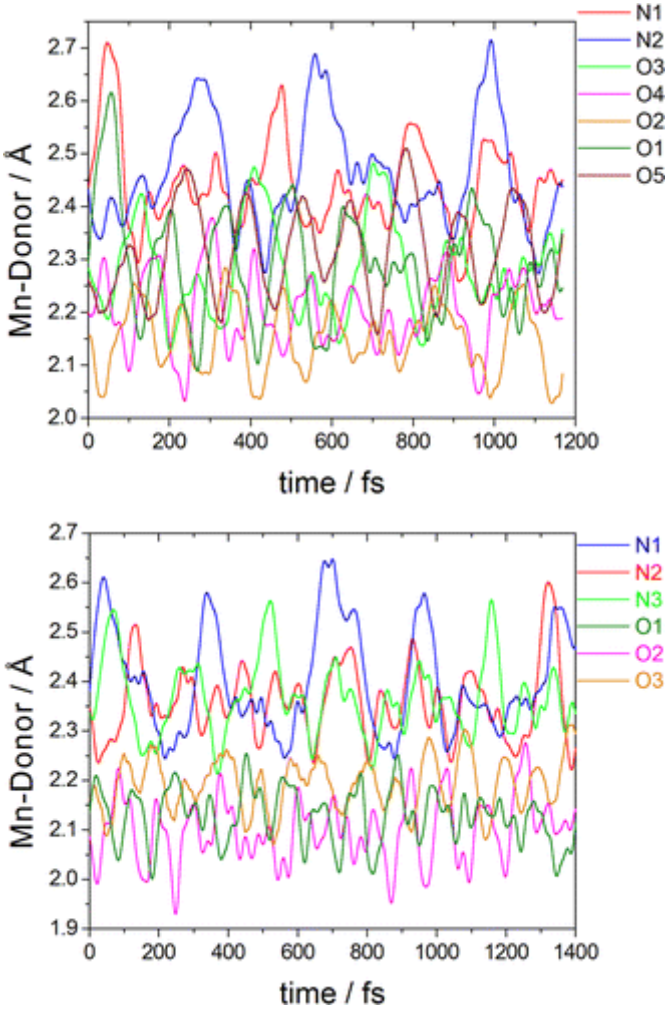

Figure 2. Calculated Mn–donor distances during the full length of the ADMP simulations performed in aqueous solution for the $[Mn(EDTA)(H_2O)]^{2-}\cdot 2H_2O$ (top) and $[Mn(MeNO2A)(H_2O)]\cdot 2H_2O$ (bottom) systems.

Given the short lengths of our MD simulations, no rotation of the complex is expected and therefore the laboratory and molecular frames can be considered identical.[28] Thus, the static ZFS parameters were estimated by diagonalization of the time average of the ZFS tensor along the trajectories obtained with ADMP calculations. The results (Table 3) suggest that the magnitude of the static ZFS does not change significantly with respect to values obtained using the minimum energy geometries. The calculated *D* parameters are little affected by the inclusion of dynamic effects, which, however, causes an increase of the rhombicity of the ZFS tensor (Table 3). This provokes changes of the sign of the *D* parameter calculated for $[Mn(EDTA)(H_2O)]^{2-}\cdot 2H_2O$ along the trajectory, which is not surprising, because it has been shown that the signs of *D* obtained with DFT methods become unreliable when $E/D > 0.2$.[63]

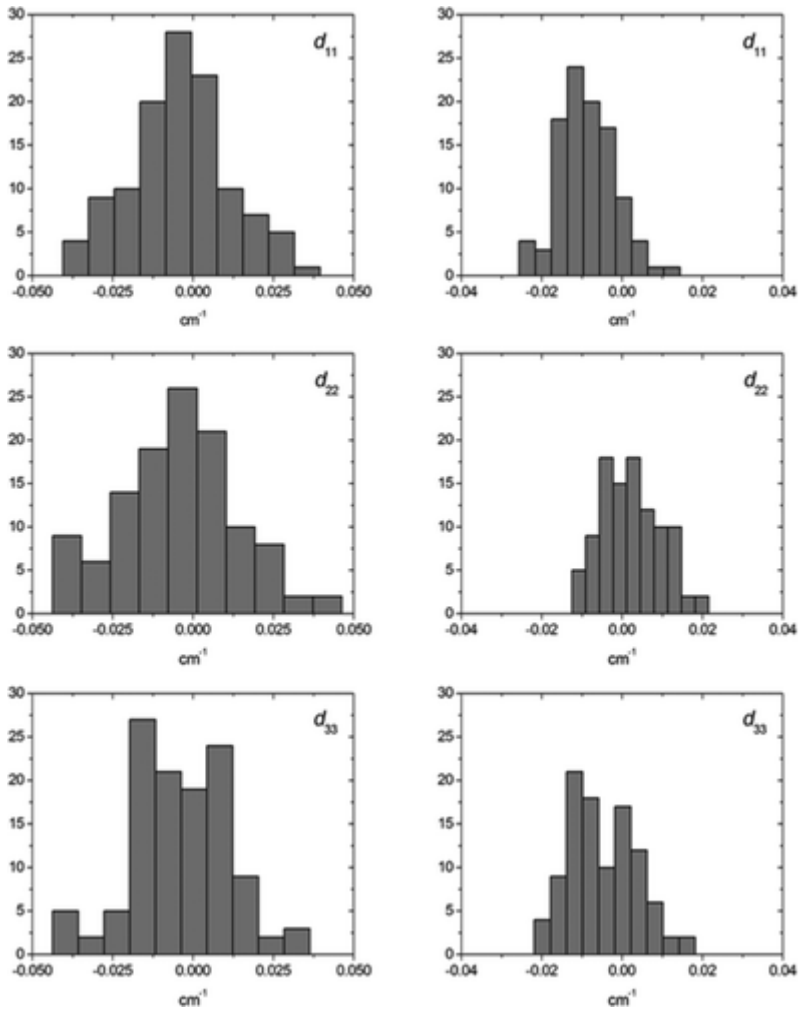

Figure 3. Distributions of d_{11}, d_{22}, and d_{33} coefficients along the trajectory of the ADMP simulations performed in aqueous solution for [Mn(MeNO2A)(H_2O)]·2H_2O (left) and [Mn(EDTA)(H_2O)]$^{2-}$·2H_2O (right).

The transient ZFS tensors were calculated along the trajectories of the ADMP simulations at the TPSS/TZVP level by subtracting the static contribution to every instantaneous ZFS tensor. Subsequently, the average of the normalized time correlation function of all nine d_{ij} coefficients $C(t)$ was calculated as proposed by Pollet:[28]

$$C(t) = \frac{1}{9}\sum_{i,j=1}^{3} \frac{\langle d_{ij}(0)\, d_{ij}(t)\rangle}{\langle d_{ij}(0)\, d_{ij}(0)\rangle} \qquad (8)$$

As for the Gd^{3+} complexes studied by Pollet, the $C(t)$ values (Figure 5) present a fast decay followed by anticorrelation. The fitting of the data to monoexponential decay functions provided the correlation times τ_c listed in Table 3. These correlation times (~0.02–0.04 ps) are somewhat shorter than those estimated by Pollet (~0.1 ps) for Gd^{3+} complexes, but very similar to that obtained for $[Ni(H_2O)_6]^{2+}$ using MD simulations (~39 fs).[73,74] The transient ZFS appears to be modulated by distortions of the metal coordination environment, resulting from fast molecular vibrations. Thus, the lower electric charge and weaker metal–donor electrostatic interactions of Mn^{2+} complexes compared to those for Gd^{3+} analogues is likely responsible for the shorter $\tau_c$values of the former. Recent measurements of the longitudinal relaxation rates

of ligand nuclei around complexed Ln^{3+} ions and previous theoretical discussion about these systems indicated that the vibrational correlation time gives a lower bound to the longitudinal electronic relaxation time values, which should not be significantly less than the inverse of the solvent collision frequency (~0.1 ps).[75,76]

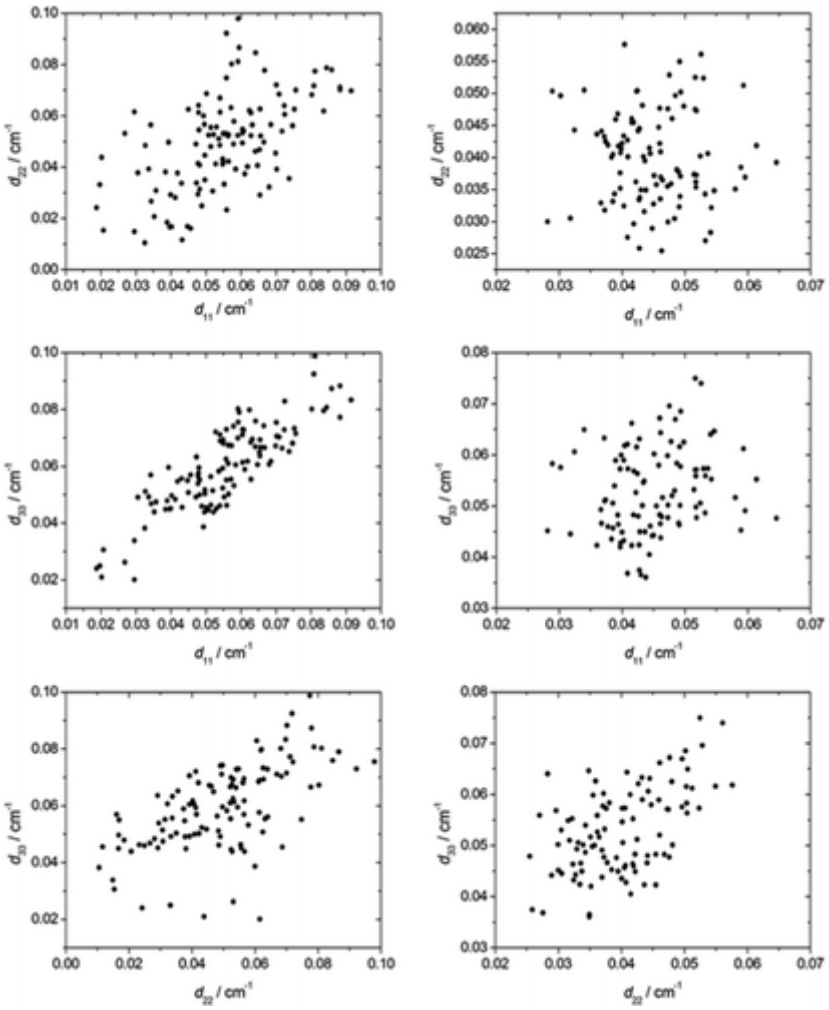

Figure 4. Correlations between the d_{11}, d_{22}, and d_{33} coefficients calculated along the trajectories of the ADMP simulations performed in aqueous solution for $[Mn(MeNO2A)(H_2O)]\cdot 2H_2O$ (left) and $[Mn(EDTA)(H_2O)]^{2-}\cdot 2H_2O$ (right).

Table 3. Static (Δ_S) and Transient (Δ_T) ZFS Obtained from Molecular Dynamics Simulations

	Δ_S/cm^{-1}	Δ_T/cm^{-1}	τ_c/ps	τ_R/ps	τ_{eff}/ps
EDTA	0.0310[a]	0.03	0.0463(9)	57[c]	28[c]
MeNO2A	0.0397[b]	0.06	0.0227(3)	36[d]	21[d]

[a]E = 0.0337 cm^{-1}; E/D = 0.3128 cm^{-1}. [b]E = 0.0457 cm^{-1}; E/D = 0.2083 cm^{-1}. [c]From ref 62. [d]From ref 30.

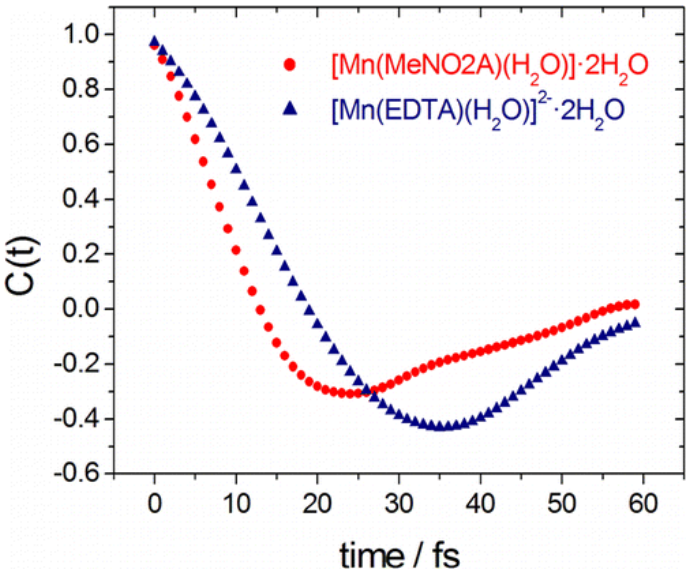

Figure 5. Normalized time autocorrelation functions of the transient ZFS contribution calculated for the Mn^{2+} complexes investigated in this work.

The transient ZFS (Δ_T) was estimated from the spread of the Δ values along the trajectories obtained with ADMP simulations (Figure 6). The ZFS energy calculated for $[Mn(MeNO2A)(H_2O)]\cdot 2H_2O$ shows important fluctuations along the trajectory of our MD simulations, whereas it fluctuates to a lesser extent for $[Mn(EDTA)(H_2O)]^{2-}\cdot 2H_2O$. As a result, the Δ_T value obtained for $[Mn(MeNO2A)(H_2O)]\cdot 2H_2O$ is about twice that of the EDTA analogue, which is in line with the broader distribution of d_{ij} values obtained for the former (Figure 3). For $[Mn(EDTA)(H_2O)]^{2-}\cdot 2H_2O$ we obtained a Δ_T value that is virtually identical to the static ZFS (Table 3). Anyhow, our calculations indicate that the static and transient ZFS have comparable values, as also suggested for Gd^{3+} complexes on the basis of EPR studies.[25,26] Interestingly, Fries and Belorizky found that $\Delta_T > \Delta_S$ for the macrocyclic $[Gd(DOTA)(H_2O)]^-$ complex, whereas the situation was reversed for the nonmacrocyclic $[Gd(DTPA)(H_2O)]^{2-}$.[25,26]

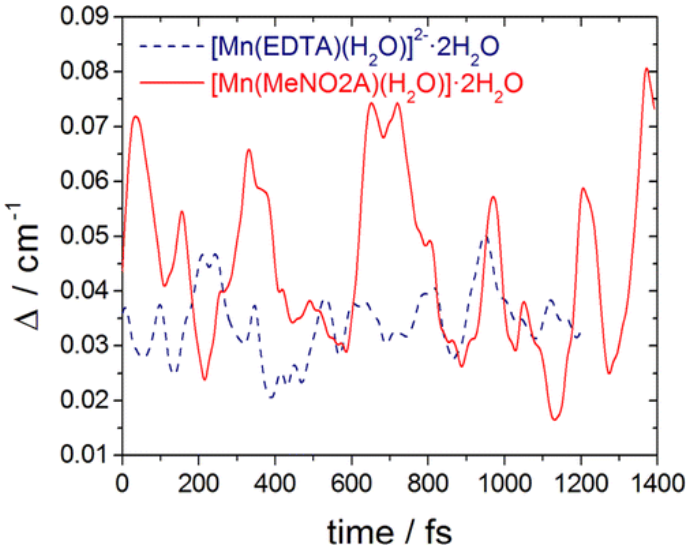

Figure 6. ZFS calculated along the trajectories of the ADMP simulations performed in aqueous solution for $[Mn(MeNO2A)(H_2O)]\cdot 2H_2O$ and $[Mn(EDTA)(H_2O)]^{2-}\cdot 2H_2O$.

Static versus Transient ZFS Relaxation

The longitudinal and transverse relaxation rates of the electron spin, $1/T_{1e}$ and $1/T_{2e}$, are often approximated by using eqs 9 and 10:[77]

$$\frac{1}{T_{1e}} = \frac{1}{25}\Delta^2\tau\{4S(S+1)-3\}\left(\frac{1}{1+\omega_s^2\tau^2}+\frac{4}{1+\omega_s^2\tau^2}\right) \quad (9)$$

$$\frac{1}{T_{2e}} = \frac{1}{50}\Delta^2\tau\{4S(S+1)-3\}\left(\frac{5}{1+\omega_s^2\tau^2}+\frac{2}{1+\omega_s^2\tau^2}+3\right) \quad (10)$$

Historically, the correlation time τ was assumed to be connected either to the molecular tumbling time τ_R or to a correlation time due to distortions of the coordination geometry of the complex, τ_v.[78] It has been found that for octahedral aqua ions the transient ZFS controls electron spin relaxation.[78] If the Redfield relaxation theory is applicable ($\Delta_s\tau_R \ll 1$), eqs 9 and 10 can be used to describe transient as well as static ZFS relaxation.[79,80] Outside the extreme narrowing limit, electron spin relaxation is expected to be a multiexponential process, although corrections for nonexponential relaxation in Mn^{2+} complexes were found to be small.[81] The parameters listed in Table 3 provide $\Delta_s\tau_R$ values of ~0.33 and 0.25 for $[Mn(EDTA)(H_2O)]^{2-}$ and [Mn(MeNO2A)(H_2O)], respectively.

Electron spin relaxation rates $1/T_{ie}$ can be calculated from the parameters in Table 3 (Figure 7). For both compounds the static contribution is dominant for $1/T_{2e}$ over the full frequency range and for $1/T_{1e}$ up to 100 MHz. At frequencies below 1 MHz all electron spin relaxation rates calculated are virtually the same.

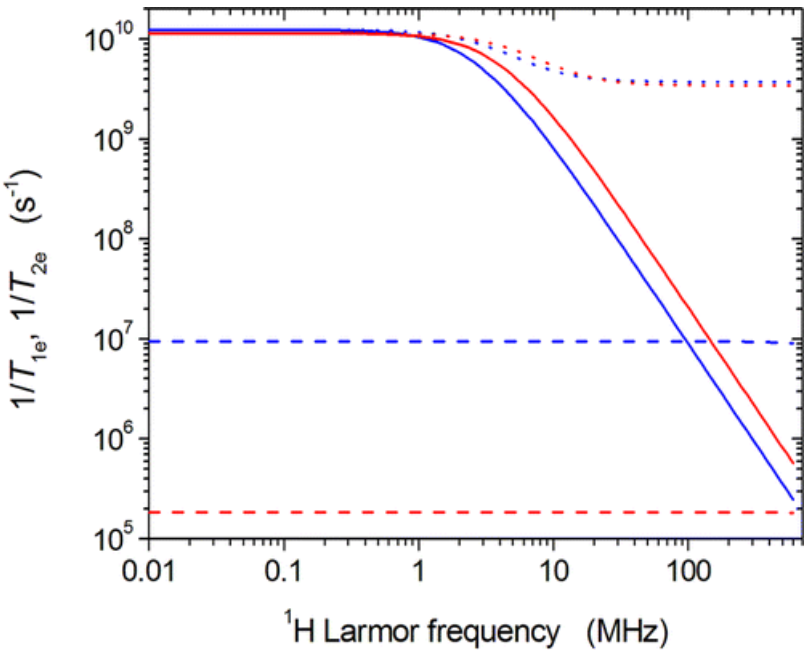

Figure 7. Electron spin relaxation rates calculated using the parameters in Table 3: $[Mn(EDTA)(H_2O)]^{2-}$, blue; [Mn(MeNO2A)(H_2O)], red. Static ZFS contribution: $1/T_{1e}$, full lines; $1/T_{2e}$, dotted lines. Transient ZFS contributions: $1/T_{1e} = 1/T_{2e}$, dashed lines.

Fries[80] proposed to use eqs 9 and 10 with an effective ZFS magnitude (Δ_{eff}) and an effective correlation time τ_{eff}. The results in Table 3 suggest that electron spin relaxation in both Mn^{2+}complexes is governed by the static ZFS modulated by molecular tumbling. Differences between τ_{eff} and the rotational correlation times τ_R can be explained by differences in sensing anisotropy in the rotational motion of the complexes. The rotational correlation times obtained from ^{1}H NMRD describe the rotational diffusion of the Mn–H vectors in the complexes, whereas the static ZFS is modulated by the rotational diffusion of the ZFS tensor. However, these deviations could also arise from the fact that eqs 9 and 10 are only valid when $\Delta_s\tau_R \ll 1$, a situation that does not strictly hold even for the small complexes studied here.

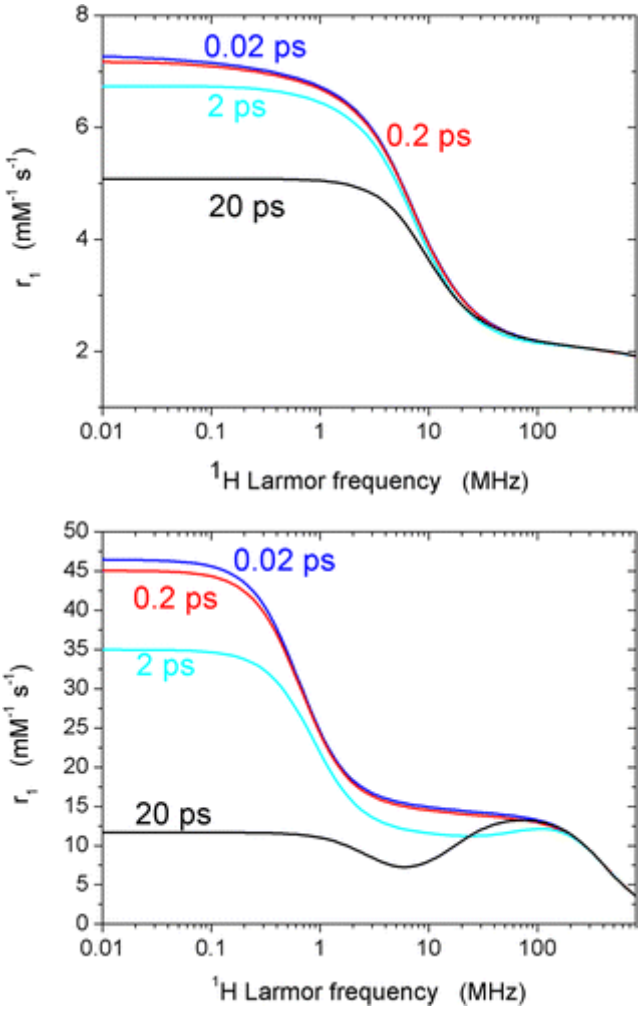

Figure 8. Top: ^{1}H NMRD profiles calculated with parameters determined for [Mn(MeNO2A)(H_2O)][44] and τ_v increasing from 0.02 to 20 ps ($\Delta^2 = 7.2 \times 10^{19}$ rad^2 s^{-2}). Bottom: ^{1}H NMRD profiles calculated with parameters determined for [Mn(MeNO2A)(H_2O)][44] except the rotational correlation time set to 500 ps and τ_v increasing from 0.02 to 20 ps.

Proton NMRD profiles for solutions of both complexes are influenced by electron spin relaxation for Larmor frequencies up to about 10 MHz.[30,62] At higher frequencies the short rotational correlation times of $\tau_R < 60$ ps are largely dominating proton relaxivity, and thus relaxivity is not affected by electron spin relaxation. This is confirmed by NMRD profiles calculated with parameters found for [Mn(MeNO2A)(H_2O)][30] and electron spin relaxation rates calculated with τ_v increasing from 0.02 to 20 ps (Figure 8). These calculations have been performed using standard Solomon–Bloembergen–Morgan (SBM) theory. We are well aware that standard SBM is in principle not valid for slowly rotating compounds. A full discussion of the validity of SBM equations can be found in the literature.[25,26,82] However, the overwhelming majority of studies of relaxation

enhancement induced by Gd^{3+}-based and Mn^{2+}-based complexes still use SBM theory to evaluate their data. Our simulations show that at $\nu > 10$ MHz the calculated relaxivity r_1 is independent of the electron spin relaxation. For slowly rotating bigger compounds this would, however, no longer be true (Figure 8, bottom). Electron spin relaxation now influences relaxivity at Larmor frequencies up to 100 MHz. However, one has to keep in mind that for slowly rotating compounds the Redfield condition is no longer valid and eqs 9 and especially eq 10 are in principle no longer valid.

Conclusions

The ZFS parameters of two Mn^{2+} complexes were computed using DFT calculations. Our results show that the TPSS functional provides the correct order of magnitude for the ZFS parameters. The transient ZFS parameters were evaluated by using MD simulations based on the ADMP approach. In spite of the relatively short time length of the MD trajectories (~1.4 ps), these simulations allowed the calculation of time correlation functions for the ZFS tensor, providing correlation times in the subpicosecond time scale (~0.02–0.04 ps). These correlation times are much shorter than those obtained from the analysis of relaxation data. Thus, the results reported in this work demonstrate that the electron spin relaxation in Mn^{2+} complexes is largely dominated by the static mechanism, which is modulated by rotation of the complex in solution.

Author Information

Corresponding Author

*C. Platas-Iglesias. E-mail: carlos.platas.iglesias@udc.es. Telephone:+34 981 167 000.

Notes

The authors declare no competing financial interest.

Acknowledgment

The authors thank Centro de Supercomputación de Galicia (CESGA) for providing the computer facilities. M.R.-F., D.E.-G., and C.P.-I. thank Ministerio de Economía y Competitividad (CTQ2013-43243-P and CTQ2015-71211-REDT) for generous financial support.

References

(1) Bertini, I.; Luchinat, C.; Parigi, G.1H NMRD Profiles of Paramagnetic Complexes and Metalloproteins *Adv. Inorg. Chem.* **2005**, 57, 105– 172, DOI: 10.1016/S0898-8838(05)57003-X

(2) *Solution NMR of Paramagnetic Molecules*; Bertini, I.; Luchinat, C.; Parigi, G.,Eds.; Elsevier: Amsterdam, **2001**.

(3) *The Chemistry of Contrast Agents in Medical Magnetic Resonance Imaging*; Merbach, A. E.; Helm, L.; Tóth, É., Eds.; Wiley: Chichester, U.K., **2013**.

(4) Caravan, P.; Ellison, J. J.; McMurry, T. J.; Lauffer, R. B. Gadolinium(III) Chelates as MRI Contrast Agents: Structure, Dynamics, and Applications *Chem. Rev*. **1999**, 99, 2293– 2352, DOI: 10.1021/cr980440x

(5) Terreno, E.; Castelli, D. D.; Viale, A.; Aime, S. Challenges for Molecular Magnetic Resonance Imaging*Chem. Rev*. **2010**, 110, 3019– 3042, DOI: 10.1021/cr100025t

(6) Peters, J. A.; Huskens, J.; Raber, D. J. Lanthanide Induced Shifts and Relaxation Rate Enhancements *Prog. Nucl. Magn. Reson. Spectrosc*. **1996**, 28, 283– 350, DOI: 10.1016/0079-6565(95)01026-2

(7) Drahos, B.; Lukes, I.; Toth, E.Manganese(II) Complexes as Potential Contrast Agents for MRI *Eur. J. Inorg. Chem.* **2012**, 1975– 1986, DOI: 10.1002/ejic.201101336

(8) Regueiro-Figueroa, M.; Rolla, G. A.; Esteban-Gómez, D.; De Blas, A.; Rodríguez-Blas, T.; Botta, M.; Platas-Iglesias, C. High Relaxivity Mn^{2+}-Based MRI Contrast Agents *Chem. - Eur. J*. **2014**, 20, 17300–17305, DOI: 10.1002/chem.201404673

(9) Rocklage, S. M.; Cacheris, W. P.; Quay, S. C.; Hahn, F. E.; Raymond, K. N. Manganese(II) *N*,*N*′-Dipyridoxylethylenediamine-*N*,*N*′-diacetate 5,5′-Bis(phosphate). Synthesis and Characterization of a Paramagnetic Chelate for Magnetic Resonance Imaging Enhancement *Inorg. Chem.* **1989**, 28, 477– 485,DOI: 10.1021/ic00302a019

(10) Grobner, T. Gadolinium - A Specific Trigger for the Development of Nephrogenic Fibrosing Dermopathy and Nephrogenic Systemic Fibrosis? *Nephrol., Dial., Transplant.* **2006**, 21, 1104– 1108, DOI: 10.1093/ndt/gfk062

(11) Ersoy, H.; Rybicki, F. J. Biochemical Safety Profiles of Gadolinium-Based Extracellular Contrast Agents and Nephrogenic Systemic Fibrosis *J. Magn. Reson. Imag*. **2007**, 26, 1190– 1197, DOI: 10.1002/jmri.21135

(12) Pan, D.; Caruthers, S. D.; Hu, G.; Senpan, A.; Scott, M. J.; Gaffney, P. J.; Wickline, S. A.; Lanza, G. M. Ligand-Directed Nanobialys as Theranostic Agent for Drug Delivery and Manganese-Based Magnetic Resonance Imaging of Vascular Targets *J. Am. Chem. Soc*. **2008**, 130, 9186– 9187, DOI: 10.1021/ja801482d

(13) Zhu, J.; Gale, E. M.; Atanasova, I.; Rietz, T. A.; Caravan, P. Hexameric Mn^{II} Dendrimer as MRI Contrast Agent *Chem. - Eur. J*. **2014**, 20, 14507– 14513, DOI: 10.1002/chem.201403883

(14) Gale, E. M.; Atanasova, I. P.; Blasi, F.; Ay, I.; Caravan, P. A Manganese Alternative to Gadolinium for MRI Contrast *J. Am. Chem. Soc.* **2015**, 137, 15548– 15557, DOI: 10.1021/jacs.5b10748

(15) Loving, G. S.; Mukherjee, S.; Caravan, P. Redox-Activated Manganese-Based MR Contrast Agent *J. Am. Chem. Soc.* **2013**, 135, 4620– 4623, DOI: 10.1021/ja312610j

(16) Hogain, D. O.; Davies, G. R.; Baroni, S.; Aime, S.; Lurie, D. The Use of Contrast Agents with Fast Field-Cycling Magnetic Resonance Imaging *Phys. Med. Biol*. **2011**, 56, 105– 115, DOI: 10.1088/0031-9155/56/1/007

(17) Solomon, I. Relaxation Processes in a System of Two Spins *Phys. Rev*. **1955**, 99, 559– 565, DOI: 10.1103/PhysRev.99.559

(18) Solomon, I.; Bloembergen, N. Nuclear Magnetic Interactions in the HF Molecule *J. Chem. Phys.* **1956**, 25,261– 266, DOI: 10.1063/1.1742867

(19) Bloembergen, N. Proton Relaxation Times in Paramagnetic Solutions *J. Chem. Phys.* **1957**, 27, 572–573,DOI: 10.1063/1.1743771

(20) Bloembergen, N.; Morgan, L. O. Proton Relaxation Times in Paramagnetic Solutions. Effects of Electron Spin Relaxation *J. Chem. Phys.* **1961**, 34, 842– 850, DOI: 10.1063/1.1731684

(21) Freed, J. H. Dynamic Effects of Pair Correlation Functions on Spin Relaxation by Translational Diffusion in Liquids. II. Finite Jumps and Independent T1 Processes *J. Chem. Phys.* **1978**, 68, 4034–4037, DOI: 10.1063/1.436302

(22) Fries, P. H.; Belorizky, E. In *The Chemistry of Contrast Agents in Medical Magnetic Resonance Imaging*; Merbach, A. E.; Helm, L.; Tóth, É., Eds.; Wiley: Chichester, U.K., **2013**; Chapter 6.

(23) Rast, S.; Borel, A.; Helm, L.; Belorizky, E.; Fries, P. H.; Merbach, A. E. EPR Spectroscopy of MRI-Related Gd(III) Complexes: Simultaneous Analysis of Multiple Frequency and Temperature Spectra, Including Static and Transient Crystal Field Effects *J. Am. Chem. Soc.* **2001**, 123, 2637– 2644, DOI: 10.1021/ja003707u

(24) Borel, A.; Clarkson, R. B.; Belford, R. L. Stochastic Liouville Equation Treatment of the Electron Paramagnetic Resonance Line Shape of an S-state Ion in Solution *J. Chem. Phys.* **2007**, 126, 054510, DOI: 10.1063/1.2433947

(25) Fries, P. H.; Belorizky, E. Determination of the Static Zero-Field Splitting of Gd3+ Complexes in Solution from the Shifts of the Central Magnetic Fields of Their EPR Spectra *ChemPhysChem* **2012**, 13, 2074– 2081,DOI: 10.1002/cphc.201200030

(26) Belorizky, E.; Fries, P. H.; Helm, L.; Kowalewski, J.; Kruk, D.; Sharp, R. D.; Westlund, P.-O. Comparison of Different Methods for Calculating the Paramagnetic Relaxation Enhancement of Nuclear Spins as a Function of the Magnetic Field *J. Chem. Phys.* **2008**, 128, 052315, DOI: 10.1063/1.2833957

(27) Fries, P. H. Computing Electronic Spin Relaxation for Gd3+-Based Contrast Agents - Practical Implementation *Eur. J. Inorg. Chem.* **2012**, 2156– 2166, DOI: 10.1002/ejic.201101430

(28) Lasoroski, A.; Vuilleumier, R.; Pollet, R. Vibrational dynamics of zero-field-splitting hamiltonian in gadolinium-based MRI contrast agents from ab initio molecular dynamics *J. Chem. Phys.* **2014,** 141, 014201, DOI: 10.1063/1.4885848

(29) Esteban-Gómez, D.; Cassino, C.; Botta, M. Platas-Iglesias, C. ^{17}O and ^{1}H Relaxometric and DFT Study of Hyperfine Coupling Constants in $[Mn(H_2O)_6]^{2+}$ *RSC Adv.* **2014**, 4, 7094– 7103, DOI: 10.1039/c3ra45721d

(30) Patinec, V.; Rolla, G. A.; Botta, M.; Tripier, R.; Esteban-Gómez, D.; Platas-Iglesias, C. Hyperfine Coupling Constants on Inner-Sphere Water Molecules of a Triazacyclononane-based Mn(II) Complex and Related Systems Relevant as MRI Contrast Agents *Inorg. Chem.* **2013**, 52, 11173– 11184, DOI: 10.1021/ic4014366

(31) Tao, J. M.; Perdew, J. P.; Staroverov, V. N.; Scuseria, G. E. Climbing the Density Functional Ladder: Nonempirical Meta-Generalized Gradient Approximation Designed for Molecules and Solids *Phys. Rev. Lett.***2003**, 91, 146401, DOI: 10.1103/PhysRevLett.91.146401

(32) Schaefer, A.; Horn, H.; Ahlrichs, R. Fully Optimized Contracted Gaussian Basis Sets for Atoms Lithium to Krypton *J. Chem. Phys.* **1992**, 97, 2571– 2577, DOI: 10.1063/1.463096

(33) Iyengar, S. S.; Schlegel, H. B.; Millam, J. M.; Voth, G. A.; Scuseria, G. E.; Frisch, M. J. Ab initio molecular dynamics: Propagating the Density Matrix with Gaussian Orbitals. II. Generalizations Based on Mass-Weighting, Idempotency, Energy Conservation and Choice of Initial Conditions *J. Chem. Phys.* **2001**, 115,10291– 10302, DOI: 10.1063/1.1416876

(34) Schlegel, H. B.; Millam, J. M.; Iyengar, S. S.; Voth, G. A.; Scuseria, G. E.; Daniels, A. D.; Frisch, M. J. Ab initio Molecular Dynamics: Propagating the Density Matrix with Gaussian Orbitals *J. Chem. Phys.* **2001**,114, 9758– 9763, DOI: 10.1063/1.1372182

(35) Schlegel, H. B.; Iyengar, S. S.; Li, X.; Millam, J. M.; Voth, G. A.; Scuseria, G. E.; Frisch, M. J. Ab Initio Molecular Dynamics: Propagating the Density Matrix with Gaussian Orbitals. III. Comparison with Born-Oppenheimer Dynamics *J. Chem. Phys.* **2002**, 117, 8694– 8704, DOI: 10.1063/1.1514582

(36) Tomasi, J.; Mennucci, B.; Cammi, R. Quantum Mechanical Continuum Solvation Models *Chem. Rev.* **2005**,105, 2999– 3093, DOI: 10.1021/cr9904009

(37) Rappe, A. K.; Casewit, C. J.; Colwell, K. S.; Goddard, W. A., III; Skiff, W. M. UFF, A Full Periodic Table Force Field for Molecular Mechanics and Molecular Dynamics Simulations *J. Am. Chem. Soc.* **1992**, 114,10024– 10035, DOI: 10.1021/ja00051a040

(38) Brancato, G.; Rega, N.; Barone, V. Unraveling the Role of Stereo-Electronic, Dynamical, and Environmental Effects in Tuning the Structure and Magnetic Properties of Glycine Radical in Aqueous Solution at Different pH Values *J. Am. Chem. Soc*. **2007**, 129, 15380– 15390, DOI: 10.1021/ja074910t

(39) Iyengar, S. S.; Schlegel, H. B.; Voth, G. A. Atom-Centered Density Matrix Propagation (ADMP): Generalizations Using Bohmian Mechanics *J. Phys. Chem. A* **2003**, 107, 7269– 7277, DOI: 10.1021/jp034633m

(40) Nam, K. Acceleration of Semiempirical Quantum Mechanical Calculations by Extended Lagrangian Molecular Dynamics Approach *J. Chem. Theory Comput.* **2013**, 9, 3393– 3403, DOI: 10.1021/ct400117k

(41) Frisch, M. J.; Trucks, G. W.; Schlegel, H. B.; Scuseria, G. E.; Robb, M. A.; Cheeseman, J. R.; Scalmani, G.; Barone, V.; Mennucci, B.; Petersson, G. A. *Gaussian 09*, Revision D.01; Gaussian, Inc.: Wallingford, CT,**2009**.

(42) Neese, F. The ORCA program system *Wiley Interdiscip. Rev.: Comput. Mol. Sci.* **2012**, 2, 73– 78, DOI: 10.1002/wcms.81

(43) Neese, F. Calculation of the Zero-Field Splitting Tensor on the Basis of Hybrid Density Functional and Hartree-Fock Theory *J. Chem. Phys.* **2007**, 127, 164112, DOI: 10.1063/1.2772857

(44) Lee, C.; Yang, W.; Parr, R. G. Development of the Colle-Salvetti Correlation-Energy Formula into a Functional of the Electron Density *Phys. Rev. B: Condens. Matter Mater. Phys.* **1988**, 37, 785– 789, DOI: 10.1103/PhysRevB.37.785

(45) Becke, A. D. Density-Functional Thermochemistry. III. The Role of Exact Exchange *J. Chem. Phys.* **1993**,98, 5648– 5652, DOI: 10.1063/1.464913

(46) Grimme, S. Accurate Calculation of the Heats of Formation for Large Main Group Compounds with Spin-Component Scaled MP2 Methods *J. Phys. Chem. A* **2005**, 109, 3067– 3077, DOI: 10.1021/jp050036j

(47) Schaefer, A.; Huber, C.; Ahlrichs, R. Fully Optimized Contracted Gaussian Basis Sets of Triple Zeta Valence Quality for Atoms Li to Kr *J. Chem. Phys.* **1994**, 100, 5829, DOI: 10.1063/1.467146

(48) Neese, F.; Wennmohs, F.; Hansen, A.; Becker, U. Efficient, Approximate and Parallel Hartree–Fock and Hybrid DFT Calculations. A 'Chain-of-Spheres' Algorithm for the Hartree–Fock Exchange *Chem. Phys.***2009**, 356, 98– 109, DOI: 10.1016/j.chemphys.2008.10.036

(49) Izsak, R.; Neese, F. An Overlap Fitted Chain of Spheres Exchange Method *J. Chem. Phys.* **2011**, 135,144105, DOI: 10.1063/1.3646921

(50) Petrenko, T.; Kossmann, S.; Neese, F. Efficient Time-Dependent Density Functional Theory Approximations for Hybrid Density Functionals: Analytical Gradients and Parallelization *J. Chem. Phys.* **2011**, 134, 054116,DOI: 10.1063/1.3533441

(51) Kossmann, S.; Neese, F. Comparison of Two Efficient Approximate Hartree-Fock Approaches *Chem. Phys. Lett.* **2009**, 481, 240– 243, DOI: 10.1016/j.cplett.2009.09.073

(52) Weigend, F.; Ahlrichs, R. Balanced Basis Sets of Split Valence, Triple Zeta Valence and Quadruple Zeta Valence Quality for H to Rn: Design and Assessment of Accuracy *Phys. Chem. Chem. Phys.* **2005**, 7,3297– 3305, DOI: 10.1039/b508541a

(53) Neese, F. Efficient and Accurate Approximations to the Molecular Spin-Orbit Coupling Operator and Their Use in Molecular g-Tensor Calculations *J. Chem. Phys.* **2005**, 122, 034107, DOI: 10.1063/1.1829047

(54) Sinnecker, S.; Rajendran, A.; Klamt, A.; Diedenhofen, M.; Neese, F. Calculation of Solvent Shifts on Electronic g-Tensors with the Conductor-Like Screening Model (COSMO) and its Self-Consistent Generalization to Real Solvents (Direct COSMO-RS) *J. Phys. Chem. A* **2006**, 110, 2235– 2245, DOI: 10.1021/jp056016z

(55) Malmqvist, P.-A.; Roos, B. O. The CASSCF State Interaction Method *Chem. Phys. Lett.* **1989,** 155, 189-194, DOI: 10.1016/0009-2614(89)85347-3

(56) Angeli, C.; Cimiraglia, R.; Malrieu, J.-P. N-Electron Valence State Perturbation Theory: A Fast Implementation of the Strongly Contracted Variant *Chem. Phys. Lett.* **2001**, 350, 297– 305, DOI: 10.1016/S0009-2614(01)01303-3

(57) Angeli, C.; Cimiraglia, R.; Malrieu, J.-P. N-Electron Valence State Perturbation Theory: A Spinless Formulation and an Efficient Implementation of the Strongly Contracted and of the Partially Contracted Variants *J. Chem. Phys.* **2002**, 117, 9138– 9153, DOI: 10.1063/1.1515317

(58) Angeli, C.; Cimiraglia, R.; Evangelisti, S.; Leininger, T.; Malrieu, J.-P. Introduction of N-Electron Valence States for Multireference Perturbation Theory *J. Chem. Phys.* **2001**, 114, 10252– 10264, DOI: 10.1063/1.1361246

(59) Angeli, C.; Cimiraglia, R. Multireference Perturbation Configuration Interaction V. Third-order Energy Contributions in the M?ller-Plesset and Epstein-Nesbet Partitions *Theor. Chem. Acc.* **2002**, 107, 313– 317,DOI: 10.1007/s00214-002-0336-z

(60) Boca, R. Zero-field Splitting in Metal Complexes *Coord. Chem. Rev.* **2004**, 248, 757– 815, DOI: 10.1016/j.ccr.2004.03.001

(61) Retegan, M.; Cox, N.; Pantazis, D. A.; Neese, F. A First-Principles Approach to the Calculation of the On-Site Zero-Field Splitting in Polynuclear Transition Metal Complexes *Inorg. Chem.* **2014**, 53, 11785– 11793,DOI: 10.1021/ic502081c

(62) Rolla, G. A.; Platas-Iglesias, C.; Botta, M.; Tei, L.; Helm, L. ^{1}H and ^{17}O NMR Relaxometric and Computational Study on Macrocyclic Mn(II) Complexes *Inorg. Chem.* **2013**, 52, 3268– 3279, DOI: 10.1021/ic302785m

(63) Zein, S.; Duboc, C.; Lubitz, W.; Neese, F. A Systematic Density Functional Study of the Zero-Field Splitting in Mn(II) Coordination Compounds *Inorg. Chem.* **2008**, 47, 134– 142, DOI: 10.1021/ic701293n

(64) Rodríguez-Rodríguez, A.; Halime, Z.; Lima, L. M. P.; Beyler, M.; Deniaud, D.; Le Poul, N.; Delgado, R.; Platas-Iglesias, C.; Patinec, V.; Tripier, R.Cyclams with Ambidentate Methylthiazolyl Pendants for a Stable, Inert and Selective Cu(II)/Cu(I) Coordination *Inorg. Chem.* **2016**, 55, 619– 632, DOI: 10.1021/acs.inorgchem.5b01779

(65) Le Fur, M.; Beyler, M.; Le Poul, N.; Lima, L. M. P.; Le Mest, Y.; Delgado, R.; Platas-Iglesias, C.; Patinec, V.; Tripier, R. Improving the Stability and Inertness of Cu(II) and Cu(I) Complexes with Methylthiazolyl Ligands by Tuning the Macrocyclic Structure *Dalton Trans.* **2016**, 45, 7406– 7420, DOI: 10.1039/C6DT00385K

(66) Ye, S.; Neese, F. How Do Heavier Halide Ligands Affect the Signs and Magnitudes of the Zero-Field Splittings in Halogenonickel(II) Scorpionate Complexes? A Theoretical Investigation Coupled to Ligand-Field Analysis *J. Chem. Theory Comput.* **2012**, 8, 2344– 2351, DOI: 10.1021/ct300237f

(67) England, J.; Bill, E.; Weyhermüller, T.; Neese, F.; Atanasov, M.; Wieghardt, K. Molecular and Electronic Structures of Homoleptic Six-Coordinate Cobalt(I) Complexes of 2,2′:6′,2″-Terpyridine, 2,2′-Bipyridine, and 1,10-Phenanthroline. An Experimental and Computational Study *Inorg. Chem.* **2015**, 54, 12002– 12018,DOI: 10.1021/acs.inorgchem.5b02415

(68) Werncke, C. G.; Suturina, E.; Bunting, P. C.; Vendier, L.; Long, J. R.; Atanasov, M.; Neese, F.; Sabo-Etienne, S.; Bontemps, S. Homoleptic Two-Coordinate Silylamido Complexes of Chromium(I), Manganese(I), and Cobalt(I) *Chem. - Eur. J.* **2016**, 22, 1668– 1674, DOI: 10.1002/chem.201503980

(69) Khan, S.; Kubica-Misztal, A.; Kruk, D.; Kowalewski, J.; Odelius, M. Systematic theoretical investigation of the zero-field splitting in Gd(III) complexes: wave function and density functional approaches *J. Chem. Phys.***2015**, 142, 034304, DOI: 10.1063/1.4905559

(70) Duboc, C.; Collomb, M.-N.; Neese, F. Understanding the Zero-Field Splitting of Mononuclear Manganese(II) Complexes from Combined EPR Spectroscopy and Quantum Chemistry *Appl. Magn. Reson.* **2010**, 37,229– 245, DOI: 10.1007/s00723-009-0085-4

(71) Pedone, A.; Biczysko, M.; Barone, V. Environmental Effects in Computational Spectroscopy: Accuracy and Interpretation *ChemPhysChem* **2010**, 11, 1812– 1832, DOI: 10.1002/cphc.200900976

(72) Borel, A.; Laus, S.; Ozarowski, A.; Gateau, C.; Nonat, A.; Mazzanti, M.; Helm, L.Multiple-Frequency EPR Spectra of Two Aqueous Gd^{3+} Polyamino Polypyridine Carboxylate Complexes: A Study of High Field Effects *J. Phys. Chem. A* **2007**, 111, 5399– 5407, DOI: 10.1021/jp066921z

(73) Odelius, M.; Ribbing, C.; Kowalewski, J. Molecular Dynamics Simulation of the Zero-Field Splitting Fluctuations in Aqueous Ni(II) *J. Chem. Phys.* **1995**, 103, 1800– 1811, DOI: 10.1063/1.469754

(74) Odelius, M.; Ribbing, C.; Kowalewski, J. Spin Dynamics Under the Hamiltonian Varying with Time in Discrete Steps: Molecular Dynamics-Based Simulation of Electron and Nuclear Spin Relaxation in Aqueous Nickel(II)*J. Chem. Phys.* **1996**, 104, 3181– 3188, DOI: 10.1063/1.471083

(75) Funk, A. M.; Fries, P. H.; Harvey, P.; Kenwright, A. M.; Parker, D. Experimental Measurement and Theoretical Assessment of Fast Lanthanide Electronic Relaxation in Solution with Four Series of Isostructural Complexes *J. Phys. Chem. A* **2013**, 117, 905– 917, DOI: 10.1021/jp311273x

(76) Fries, P. H.; Belorizky, E. Quantitative Interpretation of the Very Fast Electronic Relaxation of Most Ln^{3+} Ions in Dissolved Complexes *J. Chem. Phys.* **2012**, 136, 074513, DOI: 10.1063/1.3685584

(77) McLachlan, A. D. Line Widths of Electron Resonance Spectra in Solution *Proc. R. Soc. London, Ser. A* **1964**,280, 271– 288, DOI: 10.1098/rspa.1964.0145

(78) Rubinstein, M.; Baram, A.; Luz, Z. Electronic and Nuclear Relaxation in Solutions of Transition Metal Ions with Spin S = 3/2 and 5/2 *Mol. Phys.* **1971**, 20, 67– 80, DOI: 10.1080/00268977100100081

(79) Abernathy, S. M.; Sharp, R. R. Spin Dynamics Calculations of Electron and Nuclear Spin Relaxation Times in Paramagnetic Solutions *J. Chem. Phys.* **1997**, 106, 9032– 9043, DOI: 10.1063/1.474035

(80) Belorizky, E.; Fries, P. H. Simple Analytical Approximation of the Longitudinal Electronic Relaxation Rate of Gd(III) Complexes in Solutions *Phys. Chem. Chem. Phys.* **2004**, 6, 2341– 2351, DOI: 10.1039/b316249d

(81) Westlund, P.-O. A Generalized Solomon-Bloembergen-Morgan Theory for Arbitrary Electron Spin Quantum Number S. The Dipole-Dipole Coupling Between a Nuclear Spin I = 1/2 and an Electron Spin System S = 5/2 *Mol. Phys.* **1995**, 85, 1165– 1178, DOI: 10.1080/00268979500101741

(82) Kowalewski, J.; Kruk, D.; Parigi, G. NMR Relaxation in Solution of Paramagnetic Complexes: Recent Theoretical Progress for $S \geq 1$ *Adv. Inorg. Chem.* **2005**, 57, 41– 104, DOI: 10.1016/S0898-8838(05)57002-8